Digest Journal of Nanomaterials and Biostructures Vol. 18, No. 4, October-December 2023, p.1485-1491

Investigation of crystal structural and magnetic properties of titanium doped $Pr_{0.67}Ba_{0.33}MnO_3$ perovskite manganites

N. A. Amaran, N. Ibrahim, Z. Mohamed*
[a]*Faculty of Applied Sciences, Universiti Teknologi MARA, Shah Alam, 40450, Selangor, Malaysia*

$Pr_{0.67}Ba_{0.33}Mn_{1-x}Ti_xO_3$ (x = 0 and 0.02) were synthesized using a conventional solid-state synthesis method to investigate the effect of Ti substitution on their magnetic and electrical transport properties. All the samples were structurally evaluated by XRD diffraction Rietveld refinement method which showed an increase in unit cell volume with increasing Ni content, indicating that Ti is partially substituted at Mn. Scanning electron microscopy (SEM) and energy dispersive X-tray (EDX) are used to examine the surface morphology and identified elements in the samples' compounds. Fourier transform infrared spectroscopy (FTIR) reveals that all the samples exhibit a transmission band in the range of 590 cm^{-1} - 610 cm^{-1}. For $x = 0$, magnetization measurements showed paramagnetic (PM) to ferromagnetic (FM) transition at the transition temperature, $T_C \sim$ 213 K. For Ti-substituted samples, ferromagnetic (FM) to PM transition was reduced with Curie temperature (T_C), decreasing from 213 K ($x = 0$) to 205 K ($x = 0.02$). On the other hand, the M(H) showed the presence of a linear graph for $x = 0$ and $x = 0.02$ which may be related to the presence of paramagnetic at room temperature.

(Received July 6, 2023; Accepted November 27, 2023)

Keywords: Manganites, Rietveld refinement, Magnetic, Hysteresis loop, Paramagnetic

1. Introduction

Doped manganite oxides perovskites with the general formula, $A_{1-x}B_xMnO_3$ where A is rare earth (A = Pr, La, Sm, Nd…) and B is a divalent element (B = Sr, Ca, Ba,…), have grown in importance in recent years [1]. As a result, the development of perovskite has evolved in recent years and remains a topic of interest. This is because it is inexpensive, easily synthesized, and not harmful to the environment. Furthermore, the exceptional electrical and magnetic properties of these materials encourage researchers to investigate their use in a variety of applications such as magnetic sensors, refrigeration, supercapacitors, storage devices etc. [2][3]. The physical properties of these materials are extremely sensitive to several parameters, such as ion variation in A and B sites [4][5].

Recently, manganite doped with non-magnetic ions like Titanium at the Mn has interesting physical properties that lead to several modifications of the electrical as well as magnetic properties of the manganites [6]. Changing the temperature and composition of this material causes different phase transitions. To optimize this material, researchers must investigate the variation of electrical properties and magnetic with the temperature and doping proportion. Previous studies on the electrical properties of titanium-doped manganites have shown an improvement in the magnetotransport properties which is suggested due to its special characterization of stable tetravalent in the transition metal oxide materials. Scini et al explained that Ti doping at the B-site, resulting in a tetravalent state Ti^{4+} ([Ar], $3d^0$) [7] which causes a decrease in the number of Mn^{3+}-O-Mn^{4+}, thus may affect the mobility of charge carriers to involve in double exchange mechanism thus resulting in the change of magnetic properties. In addition, the different properties of this class of compounds can be tuned by changing the ratio of Mn^{3+} to Mn^{4+} by doping at the Mn site of the corresponding manganite [8].

* Corresponding author: zakiah626@uitm.edu.my
https://doi.org/10.15251/DJNB.2023.184.1485

As a result, it is necessary to investigate the impact of Ti doping at the Mn site on the structural and magnetic properties of $Pr_{0.67}Ba_{0.33}MnO_3$. This work presents the results of solid-state method investigations of synthesized crystalline samples of $Pr_{0.67}Ba_{0.33}Mn_{1-x}Ti_xO_3$ (x = 0, and 0.02) and an analysis of the influence of doping Ti substitution at the Mn site on the crystal structure and magnetic properties. Ti substitution at the Mn site for $Pr_{0.67}Ba_{0.33}Mn_{1-x}Ti_xO_3$ (x = 0, and 0.02) has not been reported to the author's knowledge.

2. Experimental

$Pr_{0.67}Ba_{0.33}Mn_{1-x}Ti_xO_3$ (x = 0, and 0.02) was synthesized through a standard solid-state reaction involving a high percentage of stoichiometric amounts (>99.9%) of praseodymium oxide (Pr_6O_{11}), barium carbonate ($BaCO_3$), manganese oxide (MnO_2) and titanium dioxide (TiO_2). To remove carbon, the powders were first combined in a stoichiometric ratio and ground for two hours before being calcined in air at 900 °C for twenty-four hours. After grinding, the samples were heated for 24 hours at 1000 °C and then ground again to ensure uniformity. To obtain the oxygen stoichiometry, the powders were pressed into pellets and sintered at 1100 °C for 24 hours in the air, followed by slow cooling at a rate of 1 °C/min. To achieve the desired oxygen stoichiometry, samples must be slowly cooled to recover the oxygen lost at high temperatures. The samples were analyzed with X-ray diffraction (XRD) using a PAN analytical model Xpert PRO MPD diffractometer with Cu-K radiation emitted by copper, with a characteristic wavelength of 1.5406. This was done to determine the structure and phases formed with a scattering angle range of 20° to 80°. The data was gathered by counting 18 seconds for every 0.017 degrees of rotation Using the general structure analysis systems (GSAS) programmer, the EXPGUI package, and VESTA, Rietveld refinement was performed on the XRD data. Utilizing LEO Gemini model 982 SEM equipment, the surface morphology was examined. Using energy dispersive X-ray (EDX), the elements of the compound were determined. Using the AC suscept meter system manufactured by CRYO industries, temperature-dependent measurements of AC susceptibility from 20 K to 300 K were performed. In addition, the magnetic measurements (field dependence of magnetizations) were conducted using a Quantum Design, Inc.-manufactured superconducting quantum interference device (SQUID) magnetometer setup.

3. Results

3.1. Crystal structure

Fig. 1 depicts the X-ray diffraction (XRD) patterns for $Pr_{0.67}Ba_{0.33}Mn_{1-x}Ti_xO_3$ (x = 0 and 0.02) at room temperature (a). All of the diffraction peaks in the XRD pattern are sharp, clear, and well-defined, indicating a well-crystallized sample and good preparation. Previous studies of $Pr_{0.67}Ba_{0.33}MnO_3$ reported similar diffraction peaks such as 110, 200, 022, 220, 222, 312, 400, 314, and 332 [9][1]. The position of the most intense diffraction peak shifted to lower angles with Ti substitution as indicated by the peak occurring at $2\theta \approx 33^{\circ}$. The magnified view of the most intense peak, 200, is shown in Fig. 1(b).

The XRD diffraction data were analysed using the Rietveld fitting technique to obtain structural parameters. Fitting results for both samples confirm orthorhombic symmetry with the *Pnma* space group. Table 1 shows the refined unit parameter values for $Pr_{0.67}Ba_{0.33}Mn_{1-x}Ti_xO_3$ (x = 0 and 0.02). These values indicate the quality of our refinement results.

Titanium substitution by manganese results in a small increase in the average ionic radius, $< r_B >$, which is caused by a difference in the radii of Ti^{4+} (0.605 Å) and Mn^{4+}(0.53 Å) ions [7][10]. Besides, the substitution of Ti causes an increase in unit cell volume when compared to $Pr_{0.67}Ba_{0.33}MnO_3$, which is consistent with the observed diffraction peak shifts and is similar to previous reports in $Pr_{0.75}Bi_{0.05}Sr_{0.1}Ba_{0.1}Mn_{1-x}Ti_xO_3$ [11]. On the other hand, by using the lattice parameter, space group, and Wyckoff atomic positions, the unit cell has been drawn through VESTA (Visualization for Electronic and Structural Analysis) software.

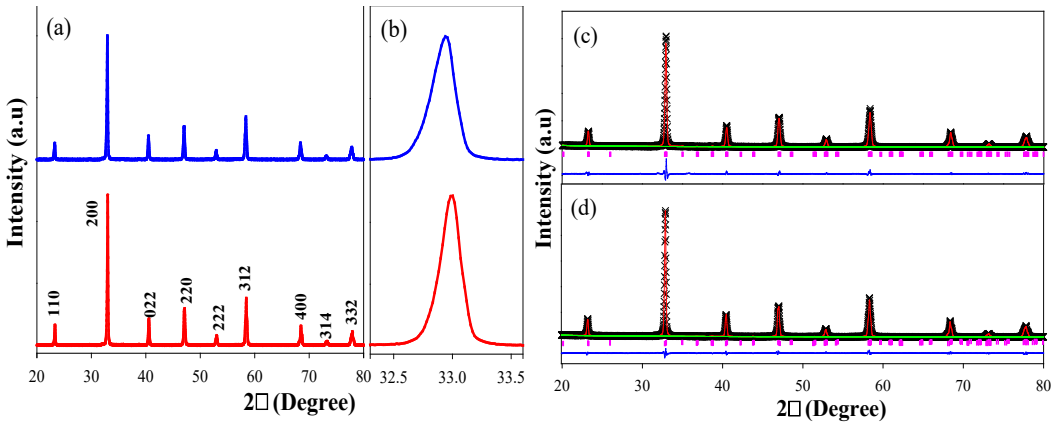

Fig. 1. (a) X-ray diffraction pattern and (b) magnified outlook of (121) peaks, and Rietveld refinement fitted patterns of $Pr_{0.67}Ba_{0.33}Mn_{1-x}Ti_xO_3$ for (c) x = 0 and (d) 0.02 manganites.

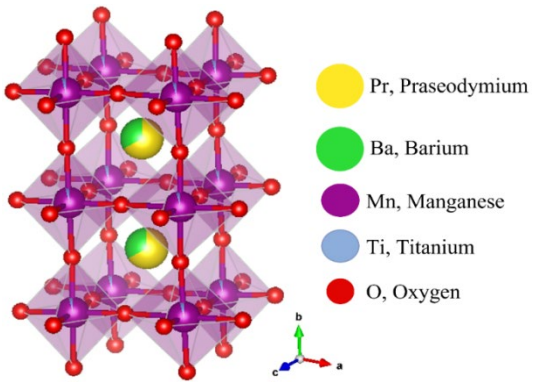

Fig. 2. Crystallographic structure for $Pr_{0.67}Ba_{0.33}Mn_{1-x}Ti_xO_3$ (x = 0.02) manganites.

Table 1. Rietveld refined parameters: lattice parameters (a, b, and c), cell volume (V) and χ^2 for $Pr_{0.67}Ba_{0.33}Mn_{1-x}Ti_xO_3$ (x = 0 and 0.02) manganites.

Parameters	***x* = 0**	***x* = 0.02**
Structure/Space group	Orthorhombic/*Pnma*	Orthorhombic/*Pnma*
a (Å)	5.504(1)	5.518(1)
b (Å)	7.778(1)	7.793(1)
c (Å)	5.528(1)	5.516(1)
V (Å^3)	236.7(8)	237.2(6)
Bond length (Å)		
2 x Mn/Ti-O_1	1.945(4)	1.948(19)
2 x Mn/Ti-O_2	1.811(3)	1.811(4)
2 x Mn/Ti-O_2	2.091(3)	2.091(4)
<Mn/Ti-O>	1.949(3)	1.950(9)
Bond Angle (◦)		
Mn/Ti-O_1-Mn/Ti	177.1(0)	177.1(1)
Mn/Ti-O_2-Mn/Ti	176.4(0)	176.4(0)
<Mn/Ti-O-Mn/Ti>	176.7(0)	176.7(1)
τ	0.942	0.942
χ^2	3.30	5.543

3.2. Scanning electron microscope (SEM)

Fig. 4 shows SEM images of $Pr_{0.67}Ba_{0.33}Mn_{1-x}Ti_xO_3$ (x = 0 and 0.02) at the same magnification of 30 μm. These images show that the unsubstituted samples form irregular shapes with different grain sizes, while the substituted sample (x = 0.02) forms more small grain sizes with close packing between the grains, which increases the number of grain boundaries. Furthermore, a reduction in average grain size with Ti substitution may be due to larger-sized ion doping at smaller ionic-sized sites. A similar finding is reported in the Ti-doped of $Pr_{0.6}Sr_{0.4}Mn_{1-x}Ti_xO_{3\pm}\delta$ manganites [12]. On the other hand, the EDX spectra revealed all of the elements with no foreign elements detected for $Pr_{0.67}Ba_{0.33}Mn_{1-x}Ti_xO_3$ (x = 0 and 0.02) manganites.

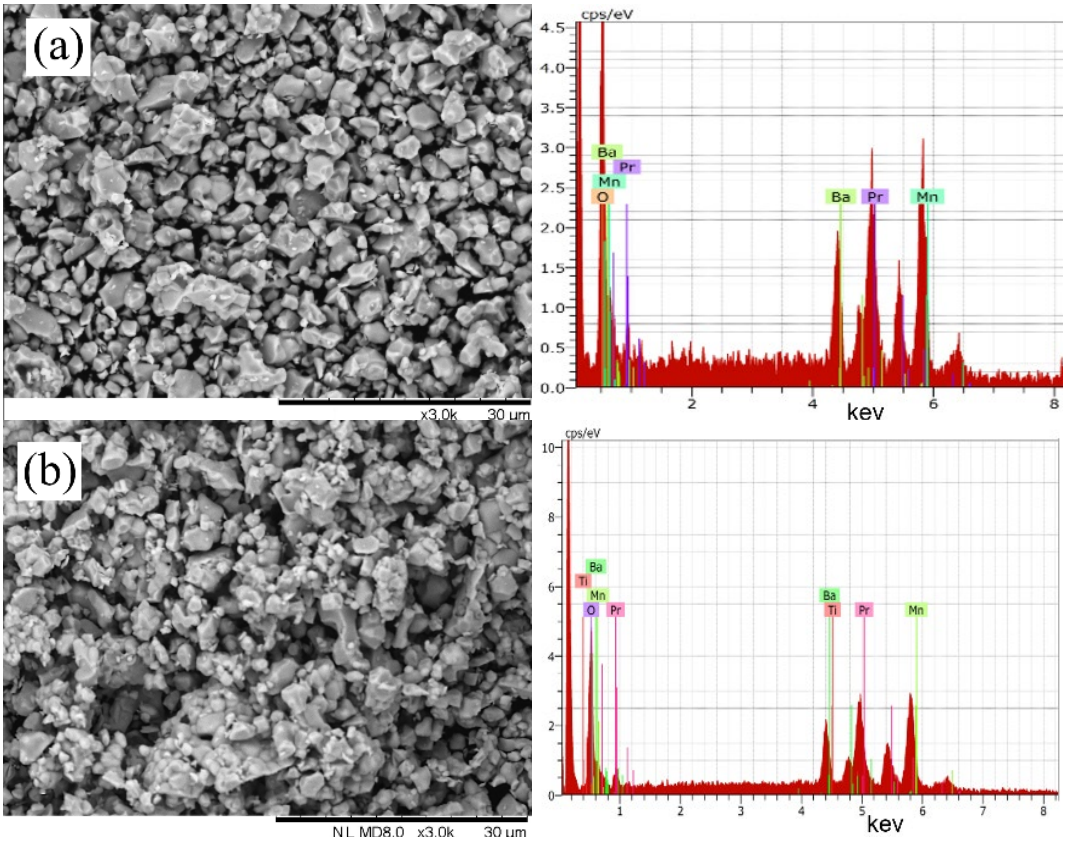

Fig. 3. SEM image and EDX spectra of $Pr_{0.67}Ba_{0.33}Mn_{1-x}Ti_xO_3$ (a) x=0 and (b) x=0.02 manganites.

3.3. Fourier Transform Infrared (FTIR)

At room temperature, the FTIR are illustrated in Fig. 4. From Fig. 4, it can be seen that both samples have a single peak at around ~600 cm^{-1}. This can be attributed to the stretching mode of the Mn^{4+} ion, which is suggested due to be caused by the Mn^{4+} moving against the oxygen in $(Mn/Ti)O_6$ octahedron [13]. Previous studies reported that this finding proves that the $(Mn/Ti)O_6$ octahedron is part of the perovskite structure, which is in line with the XRD results [14].

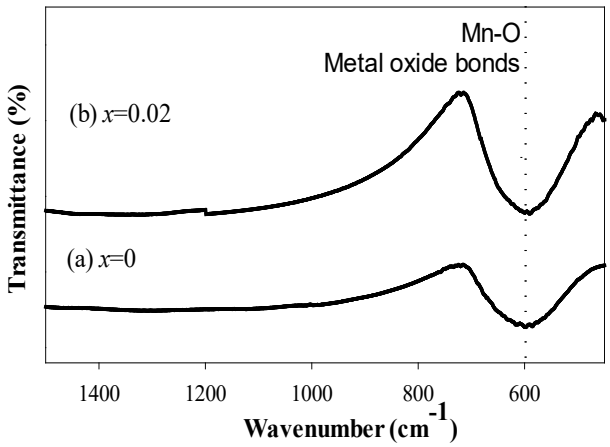

Fig. 4. FTIR spectra of $Pr_{0.67}Ba_{0.33}Mn_{1-x}Ti_xO_3$ (a) x=0 and (b) x=0.02 manganites.

3.4. Magnetic Properties

Real susceptibility for $Pr_{0.67}Ba_{0.33}Mn_{1-x}Ti_xO_3$ (x = 0 and 0.02) manganites is shown to vary with temperature in Fig. 4. The $\chi'(T)$ plots show that the unsubstituted sample (x = 0) exhibits ferromagnetic-paramagnetic (FM-PM) transition at high Curie temperature, T_C of T_C = 213 K (Table 2).

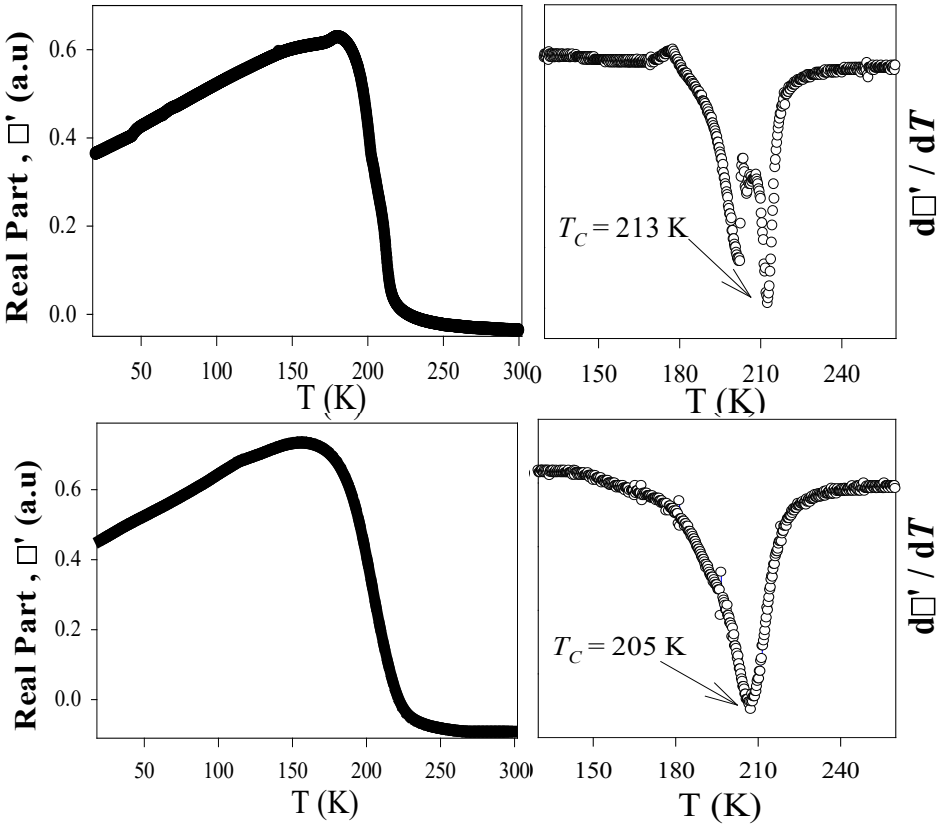

Fig. 5. (Left side) Temperature dependent of real susceptibility, χ' and (Right side) Curie temperature plot, $d\chi'/dT$ vs T for $Pr_{0.67}Ba_{0.33}Mn_{1-x}Ti_xO_3$ (x=0 and x=0.02) manganites.

Table 2. Parameter from magnetic properties for $Pr_{0.67}Ba_{0.33}Mn_{1-x}Ti_xO_3$ (x = 0 and 0.02) manganites.

Sample (x)	T_C (K)
0	213
0.02	205

The small doped with Ti (x = 0.02) caused a slight decrease of T_C which is T_C = 205 K. The T_C is the temperature at which the $d\chi'/dT$ vs. T curve has a minimum, as shown on the right side of Fig. 4. The reduction in T_C is explained by the presence of Ti^{+4} ions, which partially demolish the double exchange, DE bond between Mn^{3+}-O^{2-}-Mn^{4+} in the Mn-O plane and reduce the amount of hole electronic carrier. Furthermore, it has been discovered that in Ti-doped of $La_{0.7}Sr_{0.25}Na_{0.05}Mn_{1-x}Ti_xO_3$ [15] and $Pr_{0.75}Bi_{0.05}Sr_{0.1}Ba_{0.1}Mn_{1-x}Ti_xO_3$ [11] manganites oxides, the decrease of lattice structural such as Mn-O bond distance and Mn-O-Mn bond angle results in a weakening of the ferromagnetic, FM interaction and a reduction of T_C [6][16].

To further investigate the magnetic behavior of $Pr_{0.67}Ba_{0.33}Mn_{1-x}Ti_xO_3$ (x = 0 and 0.02) samples to the variation of the magnetic phase. Figure 5 depicts the field dependence of magnetizations of $Pr_{0.67}Ba_{0.33}Mn_{1-x}Ti_xO_3$ (x = 0 and 0.02) manganites at room temperature. The hysteresis curve of $M(H)$ curves for both samples show a linear behavior between 1.4 kOe and -1.4 kOe which is suggested a formation of PM properties of samples [17][18].

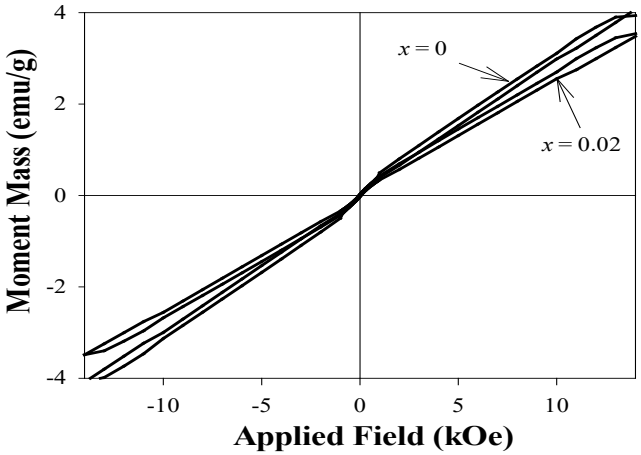

Fig. 6. Temperature dependence moment mass for $Pr_{0.67}Ba_{0.33}Mn_{1-x}Ti_xO_3$ (x=0 and x=0.02) manganites at 14 kOe.

4. Conclusions

The influence of Mn substitution by Ti on the structural, magnetic, and electrical properties of $Pr_{0.67}Ba_{0.33}Mn_{1-x}Ti_xO_3$ (x = 0 and 0.02) manganites samples prepared by conventional solid-state reaction route is investigated in this study. Rietveld refinement of XRD patterns reveals that compounds have orthorhombic unit cells with space group *Pnma*. The XRD and FTIR measurements confirm Ti incorporation into the Mn site and the resulting chemical disorder in these compounds. Furthermore, magnetic measurements show that all samples exhibit a FM-PM transition as temperature increases, which is linked to the hysteresis loop results at room temperature. The T_C of Ti-doped decrease in the temperature range of 213 K-205 K, which is suggested by the weakening of the DE interaction between Mn^{3+} and Mn^{4+} caused by the lengthening of Mn-O bond length.

Acknowledgements

The author would like to thank the Ministry of Higher Education (MOHE), Malaysia for supporting this project under the Fundamental Research Grant Scheme (FRGS) [Ref: FRGS/1/2019/STG02/UITM/02/7

References

[1] Z. Ur Rehman, M. S. Anwar, and B. H. Koo, Journal of Superconductivity and Novel Magnetism 28(5), 1629 (2015); https://doi.org/10.1007/s10948-014-2933-1

[2] R. Hamdi, J. Khelifi, I. Walha, E. Dhahri, and E. K. Hlil, Journal of Superconductivity and Novel Magnetism 32(11), 3679(2019)

[3] R. M'nassri, A. Selmi, N. C. Boudjada, and A. Cheikhrouhou, Journal of Thermal Analysis and Calorimetry 129(1), 53(2017); https://doi.org/10.1007/s10973-017-6110-1

[4] N. A. Amaran and Z. Mohamed, AIP Conference Proceedings 040028, 1(2023)

[5] N. A. Amaran, N. Ibrahim, Z. Mohamed, and A. K. Yahya, Physica B: Condensed Matter 544, 34(2018)

[6] A. Guedri, A. Omri, S. Mnefgui, and A. Dhahri, Journal of Superconductivity and Novel Magnetism 34(7), 1875(2021)

[7] K. Snini, F. Ghribi, A. Ekicibil, M. Ellouze, and L. El Mir, Journal of Materials Science: Materials in Electronics 31(23), 20657(2020); https://doi.org/10.1007/s10854-020-04596-w

[8] A. Anand, M. Manjuladevi, R. K. Veena, V. S. Veena, Y. S. Koshkid, and S. Sagar, Materials Research Bulletin 145, 111512(2022); https://doi.org/10.1016/j.materresbull.2021.111512

[9] N. A. Amaran, N. Ibrahim, and Z. Mohamed, Journal of Advanced Research in Applied Sciences and Engineering Technology 3(3), 160(2023)

[10] A. Guedri, S. Mnefgui, S. Hcini, E. K. Hlil, and A. Dhahri, Journal of Solid State Chemistry 297, 122046(2021); https://doi.org/10.1016/j.jssc.2021.122046

[11] H. E. Sekrafi, A. Ben Jazia Kharrat, N. Chniba-Boudjada, and W. Boujelben, Solid State Sciences 105, 106274 (2020)

[12] S. Khadhraoui, A. Triki, S. Hcini, S. Zemni, and M. Oumezzine, Journal of alloys and compounds 574, 290(2013); https://doi.org/10.1016/j.jallcom.2013.05.144

[13] X. Shen, G. Xu, and C. Shao, Journal of Alloys and Compounds 499(2),212(2010); https://doi.org/10.1016/j.jallcom.2010.03.169

[14] Z. Mohamed, I. S. Shahron, N. Ibrahim, and M. F. Maulud, Crystals 10(4), 295(2020); https://doi.org/10.3390/cryst10040295

[15] S. El Kossi, S. Ghodhbane, S. Mnefgui, J. Dhahri, and E. K. Hlil, Journal of Magnetism and Magnetic Materials 395, 134(2015)

[16] A. N. Ulyanov, D. S. Yang, K. W. Lee, J. M. Greneche, N. Chau, and S. C. Yu, Journal of Magnetism and Magnetic Materials 300(1), 175(2006); https://doi.org/10.1016/j.jmmm.2005.10.177

[17] M. S. Afify, M. M. El Faham, U. Eldemerdash, and W. M. A. El Rouby, Journal of Alloys and Compounds 861, 158570(2021); https://doi.org/10.1016/j.jallcom.2020.158570

[18] B. Panda, K. Lokapriya, and D. Behera, Physica B: Condensed Matter 583, 411967(2020); https://doi.org/10.1016/j.physb.2019.411967